Ultraviolet broadband light scattering for optically-trapped submicron-sized aerosol particles

Journal Article

Author(s):
David, Grégory; Esat, Kivanç (iD); Ritsch, Irina; Signorell, Ruth (iD)

Electronic Supplementary Information for PCCP article

Ultraviolet broadband light scattering for single optically-trapped submicron-sized aerosol particles

Grégory David, Kıvanç Esat, Irina Ritsch, and Ruth Signorell*

*rsignorell@ethz.ch

A. Optical trapping of the single aerosol particles

The broadband light scattering measurements are performed on single aerosol particles isolated in air by optical traps. Two types of traps are used: A quadruple Bessel beam (QBB) trap [1, 2] and a counter-propagating optical tweezer (CPT)[3-5]. Sketches of the optical layouts are provided in Fig. A.

The QBB trap (left panel in Fig. A) is composed of two perpendicularly arranged counter-propagating Bessel beam (CPBB) traps[6, 7]. The two sets of CPBB traps are obtained by splitting the beam from the trapping laser (Laser Quantum, OPUS 3 532 nm, typical power: 1000 mW) into two beams using a half-wave plate ($\lambda/2$) and a polarization beam splitter cube (PBC). From each of these two beams, a Bessel beam (BB) is formed with a 178° apex angle axicon (Altechna, 1-APX-1-H254). Each of these two BBs is then split again into two beams by $\lambda/2$ plates and PBCs to obtain the two counter-propagating BBs (BB1/BB2 and BB3/BB4), which are cross-polarized and have equal intensity. Each BB is mapped to the centre of the trapping cell by a telescope that consists of two lenses with 500 and 75 mm focal length, respectively. The core radii of the BBs in the trap centre are 3.36 µm. The typical total light intensity in the trap centre is 2.6 J s^{-1} µm^{-2} for perfect alignment.

The CPT (right panel in Fig. A) consists of two focused counter-propagating Gaussian beams (GB) of the same intensity that are cross-polarized. The radius of the incident continuous laser (Laser Quantum, OPUS 3 532 nm, typical power: 250 mW) is expanded from 0.85 to 4.25 mm with a telescope consisting of two lenses (100 and 500 mm focal length, respectively). The two counter-propagating GBs (GB1 and GB2) are obtained by splitting the expanded laser beam with a $\lambda/2$ and a PBC. Each GB is tightly focused in the centre of the trapping cell with aspherical lenses (ASL10142-532, Thorlabs, numerical

aperture (NA) = 0.145, WD = 73.7 mm). The diffraction limited radii of the two focused GBs are approximately 4.9 μm. The actual radii are expected to be slightly higher due to the optical aberrations. Assuming a diffraction limited radius, the typical total light intensity in the trap centre amounts to 6.6 J s^{-1} μm^{-2} for perfect alignment.
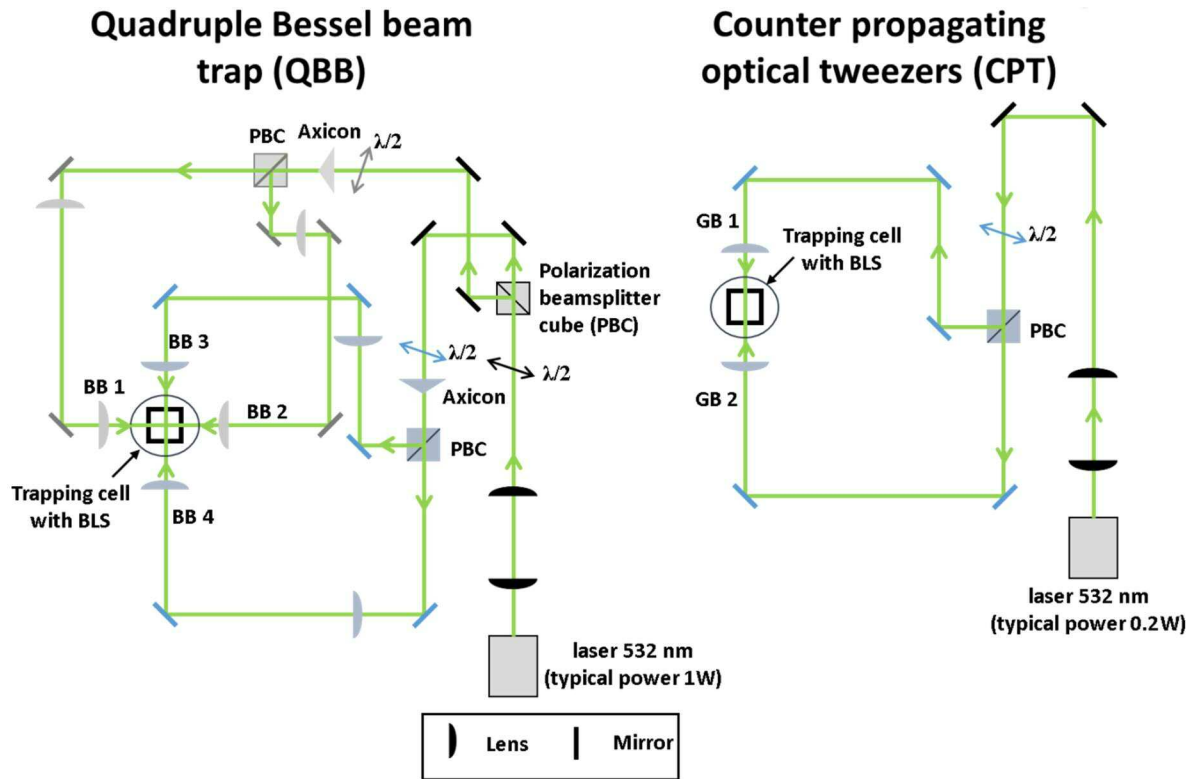
Figure A: Scheme of the QBB (left) and the CPT (right) setup.

Both traps are suitable for trapping single aerosol particles with radii in the range from a few hundred nm to several micrometers for more than several hours and performing broadband light scattering (BLS) measurements. The distance between the last optical components and the trapping centre are several centimetres for both traps. This is especially important if the conditions in the surroundings are critical (e.g. relative humidity or temperature[7]). Although both traps are suitable for BLS measurements, they have advantages and disadvantages. The QBB forms a very tightly confined trap in the range of a few tens of nanometres and trapping stability is largely insensitive to small imperfections in the alignment[2], whereas the confinement in the CPT can be on the a micrometre scale (depending on the alignment) and the trapping stability is more sensitive to imperfections in the alignment. Despite the fact that particles wobble more in the CPT, BLS measurements can still be performed yet with less accuracy. The total light intensity at the location of the trapped

particle is higher in the CPT compared with the QBB trap. This has the disadvantage of stronger heating of the particle by the trapping laser, which can lead to a decrease in the trapping stability and to a change in the physicochemical properties of the particle[8]. The advantage of the CPT over the QBB trap is the simplicity of the setup and the ease of alignment.

B. Broadband light scattering measurements

This section explains our approach to solve the inverse light scattering problem for the determination of the particle radius R and the wavelength dependent refractive index m(λ) from the BLS measurements. Previously, R and m(λ) were determined only from peak positions of the resonances in the scattering cross section[9-12] (peak position). Although this approach is computationally efficient, it involves two issues. Correctly distinguishing the peak position of resonances in noisy spectra is the first issue, especially for submicron particles. Their scattering spectra are dominated by rather broad, low mode number resonance with correspondingly smaller amplitudes and a generally low signal level; i. e. a low signal to noise ratio. This makes the identification of peak positions difficult. Secondly, the information contained in the peak shapes and the relative peak intensities is discarded if only peak positions are fitted. This can lead to seemingly good fits, which however, provide only poorly determined parameters. Obviously, a fit of the full BLS spectrum is also needed if the imaginary part of the refractive index (k) is refined together with the real part, because k strongly determines peak shapes (widths) and amplitudes. Our procedure to retrieve R and m (λ) from the raw experimental BLS spectra is composed of three steps: The derivation of the wavelength-dependent scattering cross-section from the raw BLS spectrum (Subsection B.1), the fit of the wavelength-dependent scattering cross-section using Mie theory (Subsection B.2), and the statistical analysis of the results (Subsection B.3).

B.1. Experimental scattering cross-section from BLS spectra

The signal $I_{sca}(\lambda)$ measured in a BLS experiment is proportional the intensity of the light scattered by the particle and integrated over the collected scattering angle 73.7°<θ<106.3°. $I_{sca}(\lambda)$ is proportional to the wavelength-dependent particle scattering cross-section $C_{sca,}(\lambda)$, but also depends on other wavelength-dependent experimental factors, namely the emission spectrum of the Xe lamp, the transmission and reflectivity of the optical components, and the

detection efficiency of the spectrometer. To correct for these effects we measure a "system spectrum" $I_{spec}(\lambda)$ that contains all the wavelength-dependent factors originating from the experimental setup by placing the emission and the collection optics of the BLS setup in front of each other with a 5 μm diameter pinhole in between. The wavelength-dependent experimental factors (including the emission spectrum from the Xe lamp) in general vary slowly as a function of the wavelength. While chromatic aberrations are probably not perfectly accounted for, they are also expected to impact the signal only by slow variations of its baseline. We correct for such slow intensity variations with a 3rd order polynomial $B_{exp}(\lambda)$ fitted to I_{sca}/I_{spec} over the whole wavelength range. A corrected normalized experimental scattering cross-section is then obtained as

$$C_{\exp}(\lambda) = \frac{I_{sca}(\lambda) - B_{exp}(\lambda) \cdot I_{spec}(\lambda)}{N_{exp} \cdot B_{exp}(\lambda) \cdot I_{spec}(\lambda)} \tag{B.1}$$

N_{exp} is a normalization factor so that the standard deviation of C_{exp} over the wavelength range considered is one.

B.2. Fit using Mie theory

$C_{exp}(\lambda)$ is then fitted to a normalized scattering cross-section

$$C_{sim}(\lambda) = \frac{C_{Mie}(\lambda) - B_{Mie}(\lambda)}{N_{sim} \cdot B_{Mie}(\lambda)} \tag{B.2}$$

where C_{Mie} is the cross section calculated using Mie theory and integrated over the collection angle. Calculating C_{Mie} requires the refractive index over a broad wavelength range so that the inclusion of dispersion is essential[9, 11-13]. We use the Cauchy parameterization[13, 14] referred to a reference wavelength λ_0 as described in Section 3.1 (Eq.(1)). B_{Mie} is a 3rd order polynomial fitted to C_{Mie} to remove slow intensity variations analogous to the experimental background correction B_{exp}. N_{sim} normalizes to unit standard deviation over the wavelength range considered analogous to N_{exp}.

Optimal parameters are determined by minimization of the sum of squared deviations[11, 13]:

$$SSQ(R, \mathbf{M}) = \sum_{i} \{C_{exp}(\lambda_i) - C_{sim}(\lambda_i; R, \mathbf{M})\}^2 \tag{B.3}$$

where the sum extends over the discrete values of wavelengths λ_i of the BLS spectrum. After trying out various global optimization methods, such as simulated annealing or partical swarm, a nested grid search in parameter space (R,**M**) proved to cope best with the large number of local minima in SSQ(R,**M**). Starting with a coarse grid we search a large parameter space the lowest SSQ value. The search range is then shrunk around the corresponding guess for the best (R,**M**) and the search repeated with a fine grid width. Four iterations of this procedure yield the optimal fit parameters. For example, the first loop probes R ranging from 100 to 4000 nm with a 2.5 nm resolution, m_0 ranging from 1.35 to 1.7 with a 0.015 resolution and m_1 ranging from 0 to 0.15 with a 0.0075 resolution. The final loop has a resolution of 0.5 nm in R, 0.0004 in M_0 and 0.0002 in M_1 on ranges depending on the best parameters of the third iteration. To reduce the computation time, we use a pre-calculated library of simulated spectra over a range of wavelengths (from 200 to 800 nm with a 0.1 nm resolution), particle radii (from 100 to 4000 nm with a 0.5 nm resolution), and refractive indexes (from 1.31 to 1.793 with 0.001 resolution). C_{sim} is then interpolated linearly from this library in the course of the grid search. With the current implementation of the fitting procedure, we are able to process approximately 25 spectra per hour.

B.3. Statistical analysis of the fit results

For the statistical analysis we mainly follow the procedure described by Strokotov et al.[15]. To derive a probability density in parameter space (R,M) from the function of merit SSQ(R,**M**) it is necessary to account for the serial correlation between different λ_i [16]. According to Strokotov et al.[15] and Moskalensky et al.[17] this is achieved by calculating the probability density P(**x**) with a Bayesian approach:

$$P(\mathbf{x}) = const \cdot SSQ(\mathbf{x})^{-n/2} \tag{B.4}$$

Where **x**=(R,**M**) and n is the effective number of degrees of freedom determined from the autocorrelation function[16] of $(C_{exp}(\lambda)\text{-}C_{sim}(\lambda))^2$. n is smaller than the number of wavelengths of the spectrum and takes into account the serial correlation in the fitting residuals (for details see the reference[15]). The moments of P(**x**) yield the statistical characteristics of the fit, i.e. the expectation values of the parameters $\langle\mathbf{x}\rangle$, their variances $\mathbf{F}_{var}$ and their covariances $\mathbf{F}_{cov}$:

$$\mathbf{F}_{var} = \langle(\mathbf{x} - \langle\mathbf{x}\rangle)^2\rangle \tag{B.5a}$$

$$\mathbf{F}_{cov} = \langle(\mathbf{x} - \langle\mathbf{x}\rangle)(\mathbf{x} - \langle\mathbf{x}\rangle)^+\rangle \tag{B.5b}$$

⟨ ⟩ indicates the average over P(**x**) and **x**$^+$ is the transpose of the column vector **x**. The 95 % confidence interval of the optimal parameters **x**$_{opt}$ (minimum of SSQ(**x**), Eq.(B.3)) is given by

$\Delta_{\mathbf{x}} = \left[\min\limits_{\ell \leq \ell_{max}} \mathbf{x}_{\ell}, \max\limits_{\ell \leq \ell_{max}} \mathbf{x}_{\ell} \right]$ with the condition $\sum_{\ell=1}^{\ell_{max}} P(\mathbf{x}_{\ell}) = 0.95$ for **x**$_{\ell}$ arranged in order of decreasing $P(\mathbf{x}_{\ell})$ (i.e. ℓ=1 for **x**$_{opt}$). $\Delta_{\mathbf{x}}$ defines the absolute uncertainty of **x**$_{opt}$. Finally, the correlation between two fit parameters x_i and x_j is determined by their corresponding covariance matrix element $\mathbf{F}_{cov}(x_i, x_j)$ and variances in the Pearson's product moment correlation coefficient:

$$\mathbf{F}_{corr}(x_i, x_j) = \frac{\mathbf{F}_{cov}(x_i, x_j)}{\sqrt{\mathbf{F}_{var}(x_i) \cdot \mathbf{F}_{var}(x_j)}} \tag{B.6}$$

C. Additional Figures
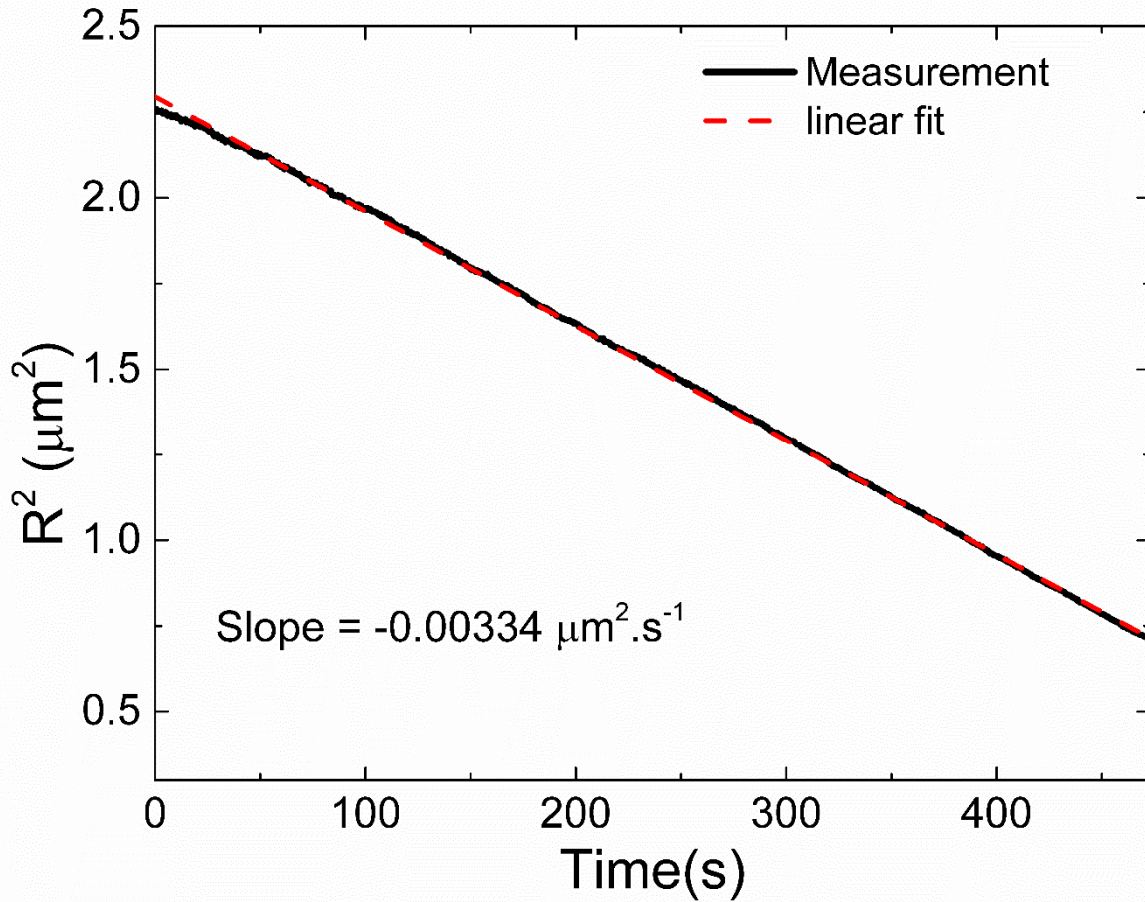
Figure B: Square of the radius (R^2) as a function of time for glycerol particles. R^2 decreases linearly with a slope of 3.34×10^{-15} m$^2 \cdot$s^{-1}.
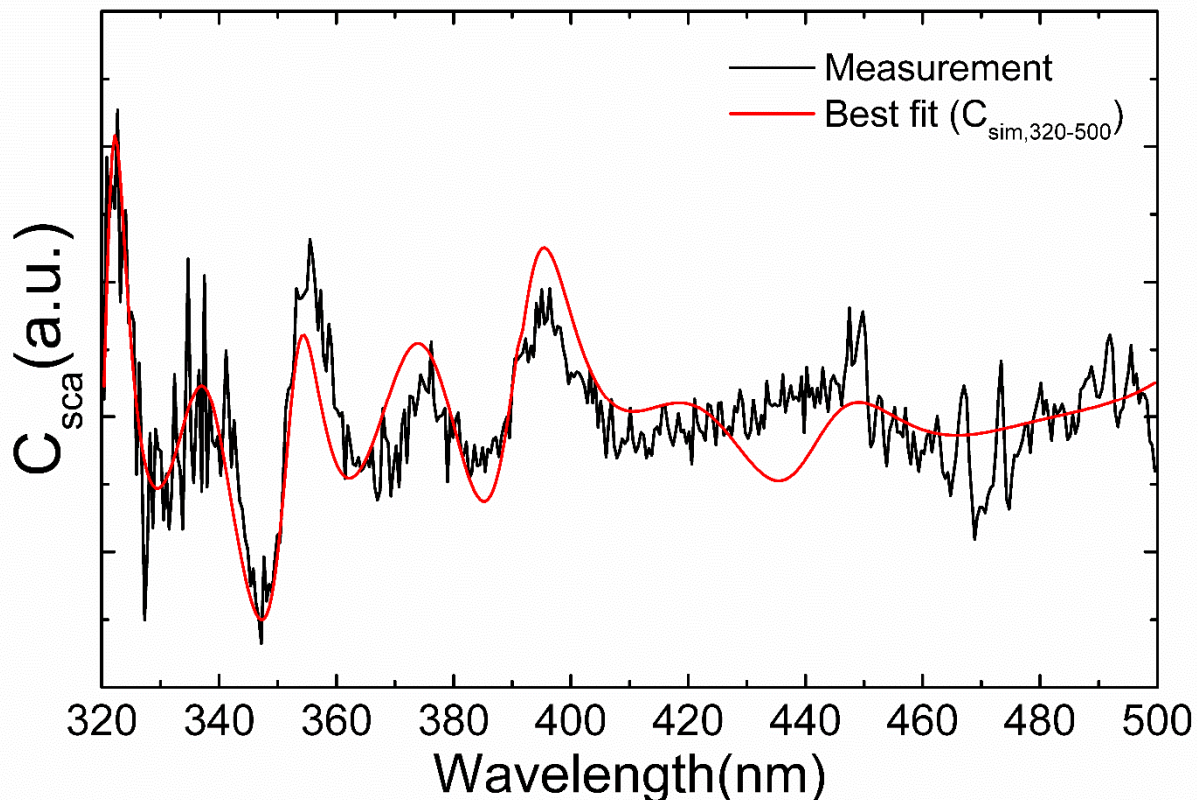
Figure C: C_{sca} as a function of the wavelength measured for the smallest oleic acid particle (see Section 4.4). The particle radius is R = 390.5 nm with Δ_R = [381.0, 400.0] nm.

References

1. I. Thanopulos, D. Luckhaus, T. C. Preston and R. Signorell, *J. Appl. Phys.*, 2014, **115**, 154304.
2. G. David, K. Esat, S. Hartweg, J. Cremer, E. Chasovskikh and R. Signorell, *J. Chem. Phys.*, 2015, **142**, 154506.
3. M. Guillon and B. Stout, *Phys. Rev. A*, 2008, **77**, 023806.
4. T. Li, S. Kheifets, D. Medellin and M. G. Raizen, *Science*, 2010, **328**, 1673-1675.
5. L. Rkiouak, M. J. Tang, J. C. J. Camp, J. McGregor, I. M. Watson, R. A. Cox, M. Kalberer, A. D. Ward and F. D. Pope, *Phys. Chem. Chem. Phys.*, 2014, **16**, 11426-11434.
6. T. Cizmàr, V. Garces-Chavez, K. Dholakia and P. Zemanek, *Proc. SPIE*, 2004, **5514**, 643-651.
7. J. W. Lu, M. Isenor, E. Chasovskikh, D. Stapfer and R. Signorell, *Rev. Sci. Instrum.*, 2014, **85**, 095107.
8. R. E. H. Miles, J. S. Walker, D. R. Burnham and J. P. Reid, *Phys. Chem. Chem. Phys.*, 2012, **14**, 3037-3047.
9. J. D. Eversole, H. B. Lin, A. L. Huston, A. J. Campillo, P. T. Leung, S. Y. Liu and K. Young, *J. Opt. Soc. Am. B*, 1993, **10**, 1955-1968.
10. A. D. Ward, M. Zhang and O. Hunt, *Opt. Express*, 2008, **16**, 16390-16403.

11. T. C. Preston and J. P. Reid, *J. Opt. Soc. Am. B*, 2013, **30**, 2113-2122.
12. L. J. Moore, M. D. Summers and G. A. D. Ritchie, *Phys. Chem. Chem. Phys.*, 2013, **15**, 13489-13498.
13. S. H. Jones, M. D. King and A. D. Ward, *Phys. Chem. Chem. Phys.*, 2013, **15**, 20735-20741.
14. J. Li, S.-T. Wu, S. Brugioni, R. Meucci and S. Faetti, *J. Appl. Phys.*, 2005, **97**, 073501.
15. D. I. Strokotov, M. A. Yurkin, K. V. Gilev, D. R. van Bockstaele, A. G. Hoekstra, N. B. Rubtsov and V. P. Maltsev, *BIOMEDO*, 2009, **14**, 064036-064036-064012.
16. G. Seber and C. Wild, *New York: Wiley*, 1989.
17. A. E. Moskalensky, M. A. Yurkin, A. I. Konokhova, D. I. Strokotov, V. M. Nekrasov, A. V. Chernyshev, G. A. Tsvetovskaya, E. D. Chikova and V. P. Maltsev, *BIOMEDO*, 2013, **18**, 017001-017001.